# J|A|C|S

Article

Aqueous Hydricity of Late Metal Catalysts as a Continuum Tuned by Ligands and the Medium

Catherine L. Pitman, Kelsey R. Brereton, and Alexander J. M. Miller*

Department of Chemistry, University of North Carolina at Chapel Hill, Chapel Hill, North Carolina 27599-3290, United States

Ⓢ *Supporting Information*

ABSTRACT: Aqueous hydride transfer is a fundamental step in emerging alternative energy transformations such as H_2 evolution and CO_2 reduction. "Hydricity," the hydride donor ability of a species, is a key metric for understanding transition metal hydride reactivity, but comprehensive studies of aqueous hydricity are scarce. An extensive and self-consistent aqueous hydricity scale is constructed for a family of Ru and Ir hydrides that are key intermediates in aqueous catalysis. A reference hydricity is determined using redox potentiometry and spectrophotometric titration for a particularly water-soluble species. Then, relative hydricity values for a range of species are measured using hydride transfer equilibria, taking advantage of expedient new synthetic procedures for Ru and Ir hydrides. This large collection of hydricity values provides the most comprehensive picture so far of how ligands impact hydricity in water. Strikingly, we also find that hydricity can be viewed as a *continuum* in water: the free energy of hydride transfer changes with pH, buffer composition, and salts present in solution.
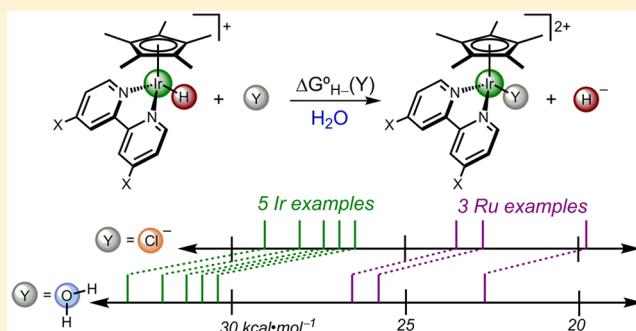
INTRODUCTION

Aqueous hydride transfer is an essential process in enzymatic catalysis in nature,[1,2] emerging fuel synthesis schemes for alternative energy,[3–6] and biphasic catalysis in chemical industry.[7,8] Hydrogenase enzymes,[9,10] for example, can produce (or split) hydrogen with exceptional rates via transition metal hydride intermediates.[1] Long-sought synthetic mimics that catalyze hydrogen evolution in aqueous solutions remain a pressing challenge.[4,11] Further, in the petrochemical industry, an aqueous-phase Rh hydride produces ~800 000 tons/year *n*-butyraldehyde for plastics.[7] Understanding and predicting the reactivity of transition metal hydrides in water will continue to gain importance as alternative feedstocks such as biomass and CO_2, which can be reduced using hydride complexes, become increasingly prevalent in the synthesis of chemicals and fuels.[6]

Thermochemical studies of metal hydrides provide a foundation for rational design of catalysts and for mechanistic studies of $2e^-$ proton-coupled electron transfer (PCET) reactions.[12,13] In acetonitrile, DuBois and Rakowski DuBois pioneered the determination of hydricity and its use as a powerful tool for reaction development in organic solvents.[14–16] In one stunning example, a decade of thermochemistry-guided catalyst design culminated in a hydrogen evolution electrocatalyst that can operate faster than hydrogenase enzymes.[17,18]

In light of the benefits that thermochemical understanding could have in the development of hydride-mediated catalysis in water, the aqueous hydricity of metal hydrides has been, until recently, surprisingly unexplored.[19] Creutz and Chou's seminal early efforts relied on experimentally challenging approach-to-equilibrium kinetics under CO_2.[20,21] Recently, the groups of Yang and Berben each reported the hydricity of one metal hydride based on the thermodynamics of H_2 cleavage reactions.[22,23] Our interest in a family of Cp*Ir-based catalysts (Cp* is pentamethylcyclopentadienyl) motivated us to develop a general and expedient method for aqueous hydricity determination in this series of complexes.

Preliminary studies on the parent complex [Cp*Ir(bpy)-(H)]$^+$ (**1H**; bpy is 2,2′-bipyridine) were stymied by the water-insolubility of the conjugate base Cp*Ir(bpy) (**1**),[24] so we charted a course utilizing carboxylate groups on the ligand to confer water solubility. We would first establish the hydricity of a reference complex using a potential–pK_a thermochemical cycle in water (Figure 1A) and then map the relative hydricity of other complexes based on hydride transfer equilibria (Figure 1B). The potential-pK_a thermochemical cycle has been used extensively in acetonitrile,[25] but has not been successfully applied in water.

The strategy depicted in Figure 1 has enabled the construction of an extensive, self-consistent aqueous hydricity scale. The broad range of Ir and Ru hydricity values reveals how the polar, protic aqueous environment impacts hydride transfer thermodynamics. Substantial shifts in the hydricity values are observed relative to acetonitrile, with electronic changes to the supporting ligand correlated strongly to the Hammett
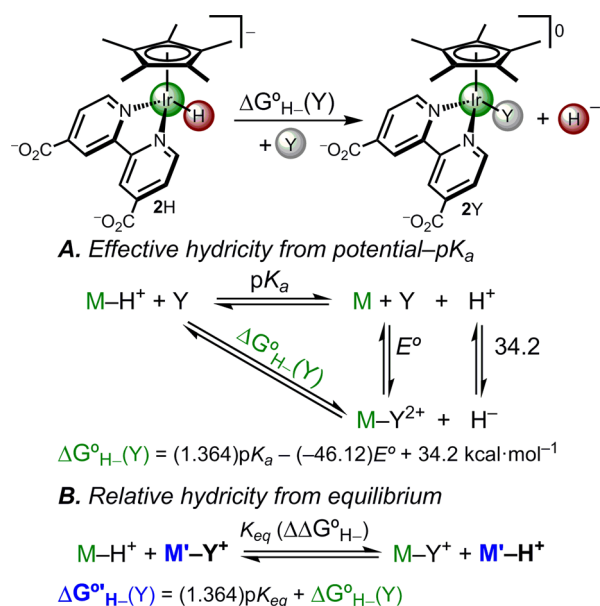
Figure 1. Scheme illustrating the hydricity of reference complex $[Cp*Ir(bpy\text{-}COO)(H)]^-$ (**2H**) and thermochemical cycles that establish aqueous hydricity of Ir and Ru hydrides.

Figure 2. (A) Spectral changes of a pH 14 solution of $[Cp*Ir(bpy\text{-}COO)(OH)]^-$ (**2OH**) as the solution potential is decreased by electrolysis to form $[Cp*Ir(bpy\text{-}COO)]^{2-}$ (**2**). (B) Absorbance at 620 nm stepping in the negative potential direction (red dots), the positive potential direction (blue dots), and the fit to the Nernst equation (dot-dashed line) giving $E^{\circ\prime} = -0.60$ V. The lack of hysteresis indicates that equilibrium was established. (C) Absorbance at 570 nm of a pH titration of $[Cp*Ir(bpy\text{-}COO)(H)]^-$ (**2H**) forming **2** (red dots) and the fit to the Henderson−Hasselbalch equation (dot-dashed line) giving $pK_a = 12.4$.

parameter σ_{p-}. A dramatic impact of water was also observed in the primary coordination sphere: a variety of suitable ligands present in aqueous media can bind the Ir or Ru centers after hydride transfer, shifting the effective hydricity substantially. Describing the complexities of hydride transfer in water allows interpretation of previously reported catalytic reactions and predictions that can guide improvements in the hydrogenation of carboxylic acids,[26] the disproportionation of formic acid to methanol,[27] and other metal hydride-mediated reactions such as H_2 evolution[28−31] and CO_2 reduction.[28,32,33]

■ RESULTS AND DISCUSSION

The first "reference" hydride investigated was $[Cp*Ir(bpy\text{-}COO)(H)]^-$ (**2H**; bpy-X = 4,4′-X-bpy), with carboxylate groups installed on the bipyridine ligand to confer good water solubility over a wide pH range, independent of metal ligation or oxidation state.[34] The hydricity of **2H** was targeted through the potential−pK_a thermochemical cycle of Figure 1A.

The reduction potential of $[Cp*Ir(bpy\text{-}COOH)(Cl)][Cl]$ (**2Cl**) was initially assessed using cyclic voltammetry (CV) in 1 M NaOH. Under these conditions, the chloride is displaced by hydroxide to form $[Cp*Ir(bpy\text{-}COO)(OH)]^-$ (**2OH**) based on NMR and MS data, and a $2e^-$ reduction forms the freely diffusing species $[Cp*Ir(bpy\text{-}COO)]^{2-}$ (**2**). Unfortunately, a large peak-to-peak separation was observed between the reduction of **2OH** and the oxidation of **2** (Figure S4). This electrochemical irreversibility, attributed to slow electron transfer or slow ligand dissociation, prevented the use of CV to determine $E_{1/2}$.[24]

Biochemists have developed an electrochemical technique suitable for quantifying reduction potentials that are hampered by slow kinetics: *redox potentiometry*.[35] Solutions varying the relative concentrations of **2OH** and **2** were prepared by partial electrolysis of a pH 14 solution of **2OH** (Figure S7). Between each stage of the electrolysis, the solution was allowed to reach equilibrium (as judged by a constant open circuit potential) and the concentrations of the Ir species were determined by UV−vis (Figure 2A). This method provided $E^{\circ\prime} = -0.60$ V for the
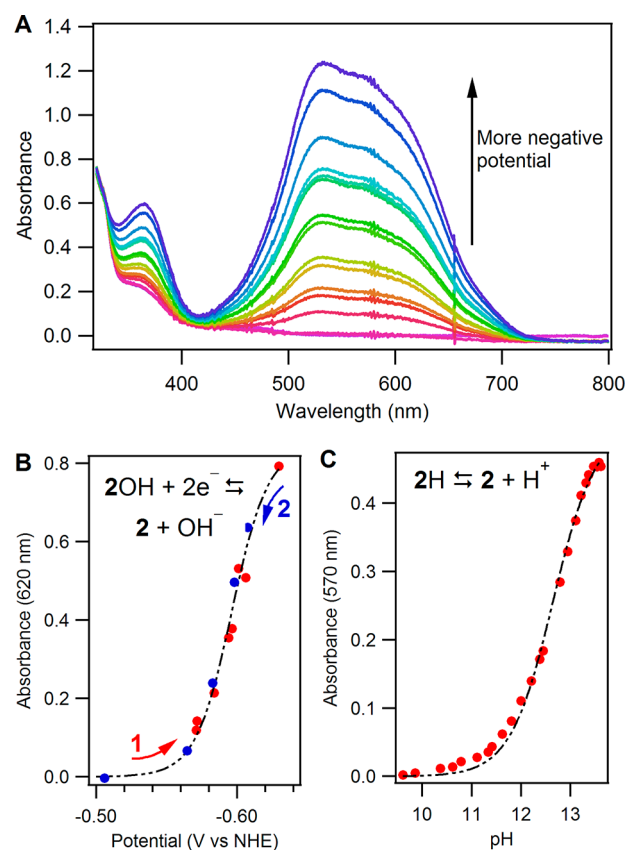
reduction of **2OH** to **2** at pH 14 (Figure 2B). As thermodynamic constants for proton reduction are determined at the standard state of pH 0,[12,19] this reduction was extrapolated to pH 0 by applying a 29.5 mV per pH unit shift ($2e^-$ reduction with loss of hydroxide), giving $E^\circ = -0.19$ V. Redox potentiometry is seldom used in organometallic chemistry,[36−38] but this method was essential to overcoming the slow kinetics that prevented the straightforward measurement of thermodynamic values.

With a reduction potential in hand, hydricity could be determined if paired with the metal hydride pK_a value. The water-soluble Ir complexes possess *several* acidic protons. Spectrophotometric titrations established the pK_a of the carboxylic acid groups in $[Cp*Ir(bpy\text{-}COOH)(OH_2)]^{2+}$ and $[Cp*Ir(bpy\text{-}COOH)(H)]^+$ as 1.9 and 2.7, respectively. The acidity of **2H** was then measured spectrophotometrically by addition of base to a yellow-orange solution of **2H** to produce a deep purple solution of **2** (Figure 2C), providing $pK_a(\mathbf{2H}) = 12.4$. The relatively acidic carboxylic acid groups provide a doubly anionic supporting ligand at pH 7 and ensure that hydride donation will not be coupled to protonation changes at the ligand.

$$\mathbf{2H} \leftrightarrows \mathbf{2} + H^+ \tag{1}$$

$$2 + OH^- \leftrightharpoons 2OH + 2e^- \tag{2}$$

$$H^+ + 2e^- \leftrightharpoons H^- \tag{3}$$

$$2H + OH^- \leftrightharpoons 2OH + H^- \tag{4}$$

The hydricity of reference complex **2H** was established by combining the pK_a of the metal hydride (eq 1), the oxidation potential of the conjugate base (eq 2), and the free energy of proton reduction to hydride (eq 3, 34.2 kcal·mol^{-1}).[19] This thermochemical cycle provides $\Delta G^\circ_{H^-}(OH)$ = 42.4 kcal·mol^{-1} (eq 4), employing the conventional standard state of pH 0.

The hydricity $\Delta G^\circ_{H^-}(OH)$ is the free energy of hydride transfer from **2H** with formation of the hydroxo complex **2OH**. Hydroxide binding is involved in the experimentally measured reduction potential, so thermochemistry involving this ligand is obtained directly. The free energy of hydride transfer from **2H** with formation of the aquo complex **2OH$_2$** can also be determined by taking into account the pK_a of **2OH$_2$** (eq 5, pK_a = 7.6 by spectrophotometric titration): $\Delta G^\circ_{H^-}(OH_2)$ = 32.0 kcal·mol^{-1}.

$$2OH + H^+ \leftrightharpoons 2OH_2 \tag{5}$$

An unusual situation arises when taking into account the metal aquo acidity: there are two *different* hydricity values for **2H**, $\Delta G^\circ_{H^-}(OH)$ and $\Delta G^\circ_{H^-}(OH_2)$. Formal hydride transfer initially results in a 16e$^-$ complex with a vacant coordination site, and this hydride dissociation process (ΔG_{H^-} in Scheme 1)

Scheme 1
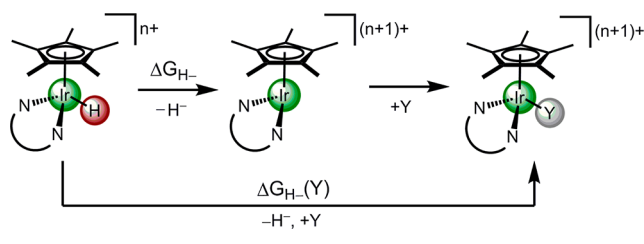
is most commonly associated with hydricity. In many cases, however, the coordinatively unsaturated complex rapidly binds a ligand (e.g., solvent or a counterion) during the net hydride transfer process. In organic solvents, solvation of the metal center after hydride transfer is commonly ignored in the thermochemistry: the activity of the solvent is taken as unity.[39−42] Water inherently contains hydroxide ions capable of binding the metal center, leading to a distinct (and pH dependent) hydricity value.

The obtained thermodynamic values $\Delta G^\circ_{H^-}(OH)$ and $\Delta G^\circ_{H^-}(OH_2)$ include the formal hydricity *and* the binding affinity for the incoming ligand (Scheme 1). A similar situation arises for acidities when, following proton loss, aggregation through hydrogen-bonding interactions (e.g., homoconjugation) influences effective acidity.[43] To distinguish the different effective hydricity values that couple hydride transfer and ligand association, the nomenclature $\Delta G^\circ_{H^-}(Y)$ is used, where Y is the incoming ligand.

Aqueous catalysis is typically carried out in the presence of various buffers and salts, and these species can also alter hydricity through metal ligation. To better understand the role of incoming ligands, we explored the effect of phosphate and chloride on hydricity. Effective hydricity values were determined by measuring the free energy of ligand exchange with **2OH$_2$** (Figure 3A) and adding that thermodynamic value
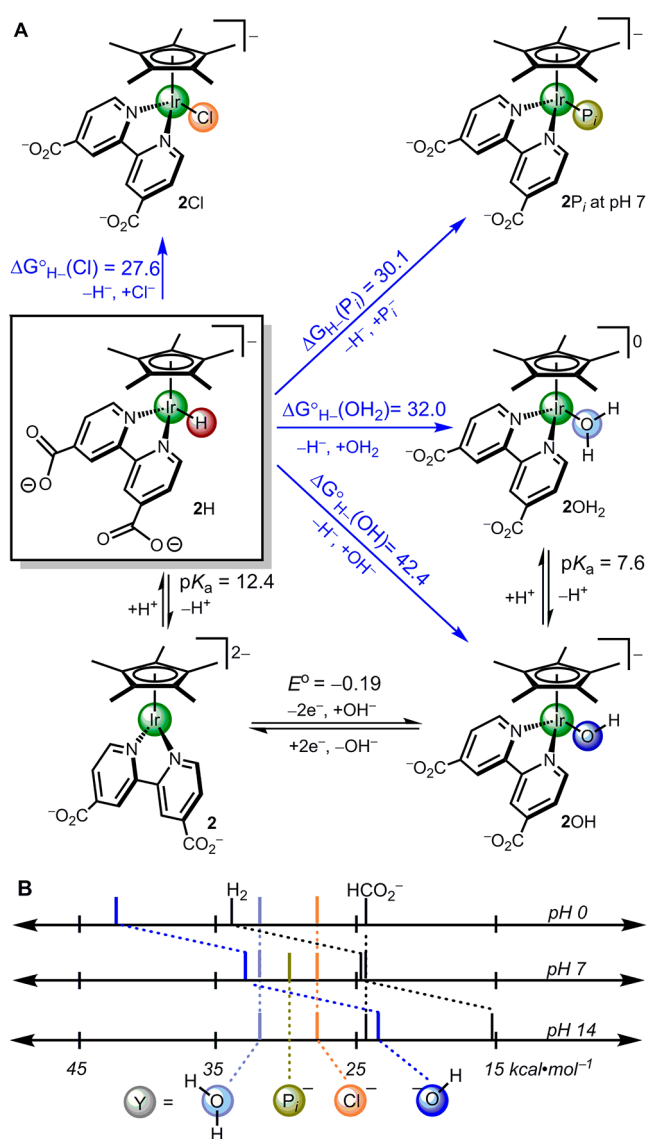

Figure 3. (A) Summary of thermochemical values of [Cp*Ir(bpy-COO)(H)]$^-$ (**2H**). Free energies (kcal·mol^{-1}) and reduction potentials (V vs NHE) are cited at the standard state of pH 0, 1 M reagents, and 1 atm gases, except for $\Delta G_{H^-}(P_i)$ that refers to pH 7. (B) Summary of the pH dependence of $\Delta G_{H^-}(Y)$ with the H$_2$O/H$_2$ and CO$_2$/HCO$_2^-$ couples.

to $\Delta G^\circ_{H^-}(OH_2)$. The relative free energy of chloride substitution was determined by NMR titration of NaCl into a pD 7 solution of **2OH$_2$**, $\Delta G_{OH_2 \rightarrow Cl}$ = −4.4 kcal·mol^{-1} (eq 6). Because ligand exchange is slow on the NMR time scale, the concentrations of the iridium species could be determined directly. The hydricity of **2H** to form the chloride product is thus $\Delta G^\circ_{H^-}(Cl)$ = 27.6 kcal·mol^{-1} (Figure 3A).

$$2OH_2 + Cl^- \leftrightharpoons 2Cl + H_2O \tag{6}$$

$$2OH_2 + P_i^- \leftrightharpoons 2P_i + H_2O \tag{7}$$

The phosphate buffer presents both H$_2$PO$_4^-$ and HPO$_4^{2-}$ ligands at pH 7, either of which can bind Ir(III).[30] Phosphate binding is apparent by NMR spectroscopy in pH 7 phosphate buffer, but rapid proton exchange prevents precise identification of the ligand protonation state. The relative binding affinity of the phosphate mixture ($\Delta G_{OH_2 \rightarrow P_i}$ = −1.9 kcal·mol^{-1} at pH 7,

eq 7) provides $\Delta G_{H^-}(P_i) = 30.1$ kcal·mol^{-1}. This hydricity is strictly accurate only at pH 7, where the measurement was made for the specific $H_2PO_4^-/HPO_4^{2-}$ mixture which P_i^- represents. The concentrations of $H_2PO_4^-$ and HPO_4^{2-} will change based on the solution pH, however, which could impact hydride transfer.

Complex **2H** is substantially more hydridic in water (smaller $\Delta G^\circ_{H^-}(OH_2)$ value) than in acetonitrile, consistent with prior studies.[22,23,41] The large differences in hydricity as a function of the ligands present in aqueous solution, however, were previously unexplored and suggest that water plays a role in hydride transfer reactions beyond simply providing a high polarity medium. Transition metal hydride transfer can be described by a *manifold of hydricity values* comprised of the heterolytic M—H bond strength (to release H$^-$) and the dative metal—ligand bond strength of any aqueous buffer components or salts.

The effective hydricity, $\Delta G^\circ_{H^-}(Y)$, is expected to be experimentally relevant to catalysis. Hydride transfer reactions for d^6 hydrides during catalysis will involve ligand association, so understanding the overall thermodynamics of that process is vital.[44] For example, in a typical pH 7 phosphate buffer solution used in photoelectrocatalytic H$_2$ evolution,[30] hydride **2H** reacts with water to release H$_2$ and generate an equilibrium mixture of Ir(III) chloride, aquo, and phosphate complexes — representing three different H$_2$ release pathways with three different hydricity values.

In water, pH also becomes an integral factor in hydricity (Figure 3B). For one, the H_2O/H_2 potential will shift to lower values as pH increases (1.36 kcal·mol^{-1}·pH^{-1}), indicating that as protons become scarcer, stronger hydrides are required to evolve H$_2$. Yet while H$_2$ is shifting, $\Delta G^\circ_{H^-}(Cl)$ and $\Delta G^\circ_{H^-}(OH_2)$ remain constant across the accessible pH range, altering net H$_2$ release thermodynamics. On the other hand, $\Delta G_{H^-}(OH)$ is influenced by pH as the concentration of ligand available for binding changes with pH. At pH 0, hydroxide ligation is unfavorable, leading to $\Delta G^\circ_{H^-}(OH) > \Delta G^\circ_{H^-}(OH_2)$; while chemical intuition might suggest that hydride transfer to form an aquo complex would be a less favorable than hydride transfer to form a complex with the more basic hydroxide ion, the extremely low concentration of hydroxide at pH 0 leads to unfavorable energetics. As the solution pH increases, however, formation of the hydroxide complex will become more favorable, and the value $\Delta G_{H^-}(OH)$ will shift smoothly. Figure 3B illustrates that at pH 14, $\Delta G_{H^-}(OH) < \Delta G_{H^-}(OH_2)$ and complex **2H** becomes a much stronger hydride donor.

Though the differences caused by incoming ligands in the aqueous medium are striking, their impact is best assessed by comparison to the effect of changing the metal center and supporting ligands. Modification of the structure of the hydride is the most common route to tune hydricity, and these synthetic strategies are typically assumed to have a greater influence than solvation of the product. To make these comparisons, we sought to explore a wider range of metal complexes and began by determining the hydricity of another soluble "reference" hydride, [(cymene)Ru(bpy-COO)(H)]$^-$ (**3H**). Hydride **3H** hails from a family of (arene)Ru(diimine) catalysts that carry out aqueous transfer hydrogenation, water splitting, and CO$_2$ reduction.[32,45,46]

The reduction potential of [(cymene)Ru(bpy-COO)(OH)]$^-$ (**3OH**) between pH 8 and 12 was measured by CV. The quasi-reversible **3OH/3** couple ($\Delta E_p = 60$ mV) shifted 26 mV per pH unit, close to the ideal value of 29.5 mV expected for a

1OH$^-$/2e$^-$ process (Figure S20). Extrapolating the trend in $E_{1/2}$ to pH 0 provided the standard reduction potential $E^\circ = -0.30$ V.[24]

Spectrophotometric titrations provided the acidity of the hydride **3H**, pK$_a$ = 11.8. From the pK$_a$ and E°, $\Delta G^\circ_{H^-}(OH) = 36.5$ kcal·mol^{-1} can be determined. Including the aquo pK$_a$ = 7.7 gives $\Delta G^\circ_{H^-}(OH_2) = 26.0$ kcal·mol^{-1}. (All the relevant pK$_a$ and $\Delta G^\circ_{H^-}$ values for this system are collected in Table S1.) The relative aquo−chloride association free energy, $\Delta G_{OH_2 \rightarrow Cl}$ = −2.9 kcal·mol^{-1}, was significantly smaller than that of the Ir complex. Taken together, the hydricity to form the chloride was determined to be $\Delta G^\circ_{H^-}(Cl) = 23.1$ kcal·mol^{-1}.

Having established two well-defined reference hydricity values, we set out to determine the hydricity of related hydrides, including the parent bpy complexes. To probe hydride transfer equilibria between Ir and Ru hydrides, however, a reliable synthetic route to these species was required. Chloride counterions were sought to increase water solubility (the previously reported PF$_6^-$ and CF$_3$SO$_3^-$ salts of **1H** were insoluble above 2 mM in water)[47] and to reduce speciation.

Electrochemical and chemical synthetic methods were developed to provide rapid access to a wide range of water-soluble metal hydrides. In a representative controlled potential electrolysis, the chloride salt of **1Cl** was converted to >20 mM of **1H** in 0.1 M pH 7 NaP$_i$. If the pH and electrolysis potential were appropriately controlled to facilitate a reduction−protonation sequence, the electrolysis method was quite general, as detailed in the Supporting Information (p. S20). Chemical syntheses were also carried out, as needed, according to a newly developed procedure. For example, reduction of the chloride salt of **1Cl** by NaBH$_4$ in 1 M NaOH resulted in precipitation of purple **1** in nearly quantitative yield. Dropwise addition of HCl·Et$_2$O to a stirring solution of **1** in Et$_2$O prompted precipitation of the golden yellow chloride salt of hydride **1H**. This procedure is also generally applicable, except when the metal hydride cannot be deprotonated in water or the conjugate base does not precipitate from water (see Supporting Information p. S20 for full details).

With a collection of hydride complexes (see Figure 4 for numbering scheme), relative hydricity could be determined by mixing a hydride donor and a hydride acceptor and allowing the system to reach an equilibrium distribution of both hydrides and acceptors. The concentration of each species was determined by NMR, and the equilibrium constant provided the difference in hydricity ($\Delta\Delta G^\circ_{H^-}$) between the two complexes, according to Figure 1B.[48] Figure 4 depicts the relative hydricity of each hydride complex, with each reaction representing a hydride−chloride exchange.

In a representative hydride equilibration, a solution of **2Cl** in pD 7 0.1 M NaP$_i$ (produced electrochemically in 84% yield, with 16% unreacted **2Cl**) was mixed with **1Cl**. After the reaction was allowed to reach equilibrium, the concentrations of **1H**, **1Cl**, **2H**, and **2Cl** were measured by ^{1}H NMR spectroscopy. The equilibrium constant, $K_{eq} = 0.35$, provided $\Delta\Delta G^\circ_{H^-} = 0.6$ kcal·mol^{-1} (eq 8) and established the hydricity of **1H** in a single experiment: $\Delta G^\circ_{H^-}(Cl) = 27.0$ kcal·mol^{-1}. It is noteworthy that equilibration was established in <15 min, and though our present focus is on *thermodynamic* hydricity, this contrasts with the frequently kinetically slow hydride transfer reactions reported in acetonitrile.[41,48]

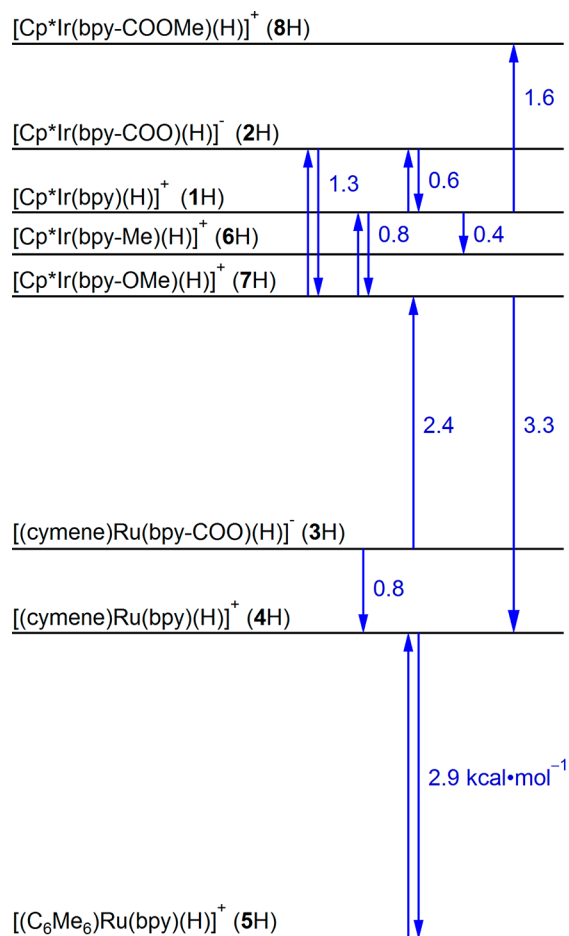$$\textbf{2H} + \textbf{1Cl} \rightleftharpoons \textbf{2Cl} + \textbf{1H} \qquad (8)$$

Figure 4. Relative hydricity values of Ir and Ru complexes (blue). The equilibria used to determine hydricity are represented by blue arrows.

A series of hydride transfer equilibrium experiments established the relative hydricity scale of Figure 4. Equilibrium could be established from either direction to give $\Delta\Delta G^{\circ}_{H^-}$ values that were identical within experimental uncertainty (± 0.1 kcal·mol^{-1}, see Supporting Information p. S36 for full experimental details). Hydricity values were determined from these relative hydricities by comparison to the $\Delta G^{\circ}_{H^-}$(Cl) of reference **2H** for Ir complexes and reference **3H** for Ru complexes, and the scale is self-consistent within the ± 1 kcal·mol^{-1} estimated uncertainty of the measurements.[25,48,50] The $\Delta G^{\circ}_{H^-}$(OH$_2$) for all complexes was determined by measuring the aquo-chloride relative association energy of each of these species (Table 1).

Table 1. Aquo-Chloride Association Free Energy and Hydricity to Form Ligated Products in kcal·mol^{-1}

complex	$\Delta G^{\circ}_{H^-}$(Cl)	$\Delta G^{\circ}_{H^-}$(OH$_2$)	$\Delta G_{OH_2 \rightarrow Cl}$
1	27.0	31.5	−4.5
2	27.6	32.0	−4.4
3	23.1	26.0	−2.9
4	22.3	25.6	−3.3
5	19.4	22.9	−3.5
6	26.6	31.1	−4.5
7	26.2	30.8	−4.6
8	28.6	33.4	−4.7

Our values are also consistent with one of the few other well-defined hydricity values available in the literature: the hydricity of $[(C_6Me_6)Ru(bpy)(H)]^+$ (**5H**) with formation of **5**OH$_2$ was reported by Creutz, $\Delta G^{\circ}_{H^-}$(OH$_2$) = 22.2 kcal·mol^{-1},[19,21] which we independently determined to be $\Delta G^{\circ}_{H^-}$(OH$_2$) = 22.9 kcal·mol^{-1}.

In Figure 5, our continuum of hydricity values is contextualized against previously reported hydricity values $(\Delta G^{\circ}_{H^-}$(OH$_2$)) for transition metal hydrides and substrates relevant to alternative energy pursuits (H$^+$ and CO$_2$). The previously reported Ru and Rh complexes are aquated after hydride transfer. The two parallel scales illustrate the role of the ligand bound to the product and the influence of changes to the supporting ligands or metal center. In general, the hydricity values are much smaller in water than in acetonitrile.[41,47]

Electron-donating groups promote hydride transfer, as evidenced by a strong correlation between $\Delta G^{\circ}_{H^-}$(Cl) and the Hammett parameter σ_{p-} (Figure 6).[51] The Ir and Ru catalysts investigated herein become better hydride donors (lower $\Delta G^{\circ}_{H^-}$) with increasing electron density. Hydricity is moderated by electronic effects: increasing electron density increases pK_a and shifts E° more negative which raise and lower hydricity, respectively. In fact, other systems have been found to be more influenced by the ligand bite angle than by electronics.[25] The ease with which each ligand can stabilize increased electron density is reflected in electronic spectroscopy: hydricity is correlated to the metal-to-ligand charge-transfer band around 400 nm that is present in each of the Ir hydride complexes (Figure S42). Interestingly, the *activity* of aqueous hydrogen evolution catalysis involving Cp*Ir-based catalysts also correlates with electron-donating ability of the bipyridine ligand,[31] suggesting that perhaps the increase in rate is due to an increase in the hydricity of the metal hydride intermediate.

Electronic changes to the bipyridine ligands affect the *acidity* of the metal hydride more dramatically than the hydricity. The hydricity difference between methoxy-substituted **7H** (pK_a > 14) and methylester-substituted **8H** (p$K_a \sim 5$, estimated from CV, see Supporting Information p. S4) is only 2.4 kcal·mol^{-1}, while the acidity difference between these complexes spans ~ 9 orders of magnitude (~ 12 kcal·mol^{-1}).

Ligand effects on hydricity were more pronounced when changes were made to the arene rings.[48] Cymene complex **4H** and hexamethylbenzene complex **5H** displayed a ~ 3 kcal·mol^{-1} difference in hydricity that is larger than observed for bpy ligand modifications, but of a similar magnitude to the effect of chloride ligation. These differences warrant further studies into possible steric effects in these thermodynamic hydricity values.

The emerging picture of aqueous hydricity tunable by both ligands *and* the medium could impact catalysis. Electrocatalytic hydrogen evolution in water is usually carried out with pH-stabilizing buffer bases,[4] and water splitting schemes that employ salt water must wrestle with an abundance of chloride,[52,53] which would lead to a ~ 5 kcal·mol^{-1} difference in the hydricity of Ir catalysts. The hydricity trends in Figure 5 also predict the pH at which H$_2$ evolution will occur, as a function of the ligand electronics and the presence of incoming ligands in solution. All of the complexes investigated, for example, are predicted to produce H$_2$ at pH 0 ($\Delta G^{\circ}_{H^-}$ < 34.2 kcal·mol^{-1}), but at pH 10 only Ru complex **5H** is thermodynamically capable of forming H$_2$ (and only at high chloride concentration). Under basic conditions, hydroxide ligation could also start to impact hydride transfer reactivity.
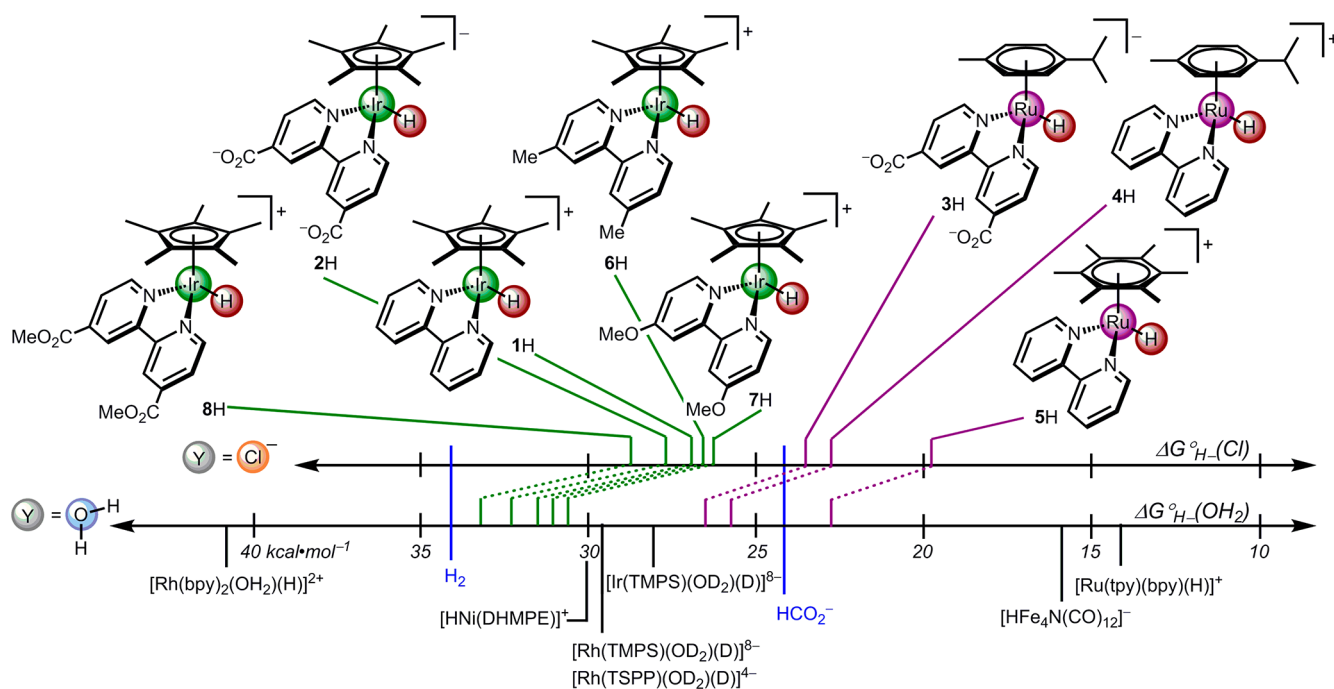
Figure 5. Aqueous hydricity scale of the complexes we report along with those previously reported in the literature. Y represents the incoming ligand such that the top scale shows $\Delta G°_{H^-}(Cl)$ and the bottom scale shows $\Delta G°_{H^-}(OH_2)$. TSPP = tetra(p-sulfonatophenyl)porphyrin; TMPS = tetrakis(3,5-disulfonatomesityl)porphyrin; tpy = terpyridine; DHMPE = 1,2-bis(dihydroxymethylphosphino)ethane.[19,22,23,49]
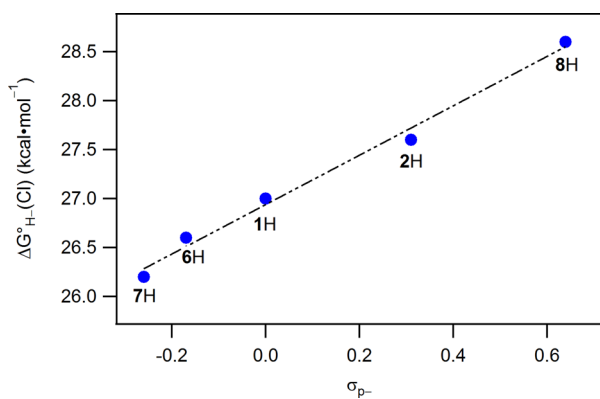

Figure 6. Correlation between σ_{p^-} and $\Delta G°_{H^-}(Cl)$.

The ability of a hydride to reduce CO_2 to formate at pH 0 can also be predicted by inspection of Figure 5. Species more hydridic than formate ($\Delta G°_{H^-} < 24.1$ kcal·mol^{-1}) are thermodynamically capable of CO_2 reduction. An intriguing prediction arises from Figure 5: CO_2 reduction by hydride transfer from (cymene)Ru complexes **3H** and **4H** should be unfavorable in unbuffered water and favorable only when chloride anion is present. The less hydritic hydrides would require increased CO_2 pressure to enable hydride transfer to CO_2. In a prior report of CO_2 hydrogenation, the Ir hydride **1H** underwent slow, rate-limiting hydride transfer to CO_2, while the Ru hydride **5H** transferred hydride sufficiently quickly that H_2 cleavage became rate-limiting.[32] Our studies show that **5H** is more hydridic than the parent Ir complex **1H**; the hydricity scale correctly predicts that **5H** will more readily hydrogenate CO_2 (and less readily cleave H_2).

CONCLUSIONS

A general strategy for the determination of hydricity in water is presented. Comparisons across a range of well-known catalytic intermediates were enabled by an electrochemical technique well suited to the complications of water and by new synthetic routes to water-soluble hydrides. Thermodynamic hydricity in water is not only influenced by the supporting ligands, but also by the ligating species present in aqueous media. Rather than a single value defined in terms of the hydride donor, a continuum of hydricity values should be considered. Being cognizant of the resulting product after hydride transfer makes direct comparisons between catalysts and conditions possible.

The hydricity scales suggest new strategies in aqueous catalysis. The synthetic chemist instinctively tunes catalysts through ligand modifications, but tuning the medium itself can also effect changes in hydricity. The present findings will guide further thermodynamic studies of PCET events in water and guide aqueous catalyst development.

EXPERIMENTAL SECTION

General Considerations. Procedures were carried out under nitrogen except where noted. All solutions containing metal hydride species were protected from ambient light to prevent excited state reactions.[30] All reagents were commercially available and used without further purification. Commercial HPLC-grade water was used as a solvent, and organic solvents were dried and degassed with argon using a Pure Process Technology solvent system. Deuterated solvents were purchased from Cambridge Isotope Laboratories, Inc. Electrochemical experiments were performed on a Pine WaveNow potentiostat or Pine WaveDriver bipotentiostat controlled by Aftermath software. Details on specific electrochemical experiments are described below. Solution pH was recorded using an OrionStar A111 pH meter with a Beckman-Coulter, Hanna, or Hach ISFET pH probe. UV−vis spectra were obtained using an Ocean Optics USB2000+ spectrometer with a DT-MINI-2GS deuterium/tungsten halogen light source controlled by OceanView software.

NMR spectra were obtained on 400, 500, or 600 MHz spectrometers. ^{1}H NMR spectra were referenced to the residual solvent signals (or dioxane or NaOTs as an internal standard in D$_2$O).[54] Spectra were processed using the MestReNova software suite from Mestrelab Research S. L. The solution acidity in NMR experiments is reported as pD, obtained by addition of +0.4 to the reading of a pH electrode that was calibrated using H$_2$O standards.[55]

ESI-MS were obtained on a Thermo Scientific LTQ FT-ICR MS with samples introduced either through direct infusion or by LC. Inductively coupled plasma-mass spectrometry (ICP-MS, Agilent Technologies 7500x series) was employed to determine the precise Ir and Ru concentrations in UV−vis samples (for molar extinction coefficient determination), with the aid of a calibration curve for 10−500 ppb Ir and Ru.

Electrochemistry. Electrochemical experiments were carried out with carbon working electrodes, platinum wire counter electrodes, and Ag/AgCl (3 M NaCl) reference electrode in a small glass tube fitted with a Vycor glass frit. Solutions were thoroughly degassed by sparging with nitrogen for at least 15 min before beginning an experiment. All potentials are reported relative to NHE, with values obtained by adding 0.21 V to the experimentally observed potential vs Ag/AgCl.[56]

Cyclic voltammetry experiments were carried out with a glassy carbon working electrode (polished with 0.05 μm alumina powder between scans) in an undivided cell. Controlled potential electrolysis experiments were carried out with reticulated vitreous carbon (RVC) as the working electrode separated from the counter electrode and reference electrodes by a fine frit in an H-cell.

Potentiometric experiments were performed in a custom-made three-compartment cell divided by fine frits and with a 10 mm × 10 mm Pyrex glass cuvette affixed to the central working electrode chamber (Figure S1). The solution was stirred at the base of the cuvette and by a slow bubble of N$_2$ through the length of the cuvette to ensure sufficient mixing near the electrode. An RVC electrode was used as the working electrode for both the electrolysis and open circuit potential experiments. Reduction and oxidation of the analyte was achieved via short periods of electrolysis, and after each pulse of current, sufficient time was allowed for the solution components to come into equilibrium (typically 5−10 min) as judged by an unchanging open circuit potential over 30 s. After equilibrium was established, UV−vis spectra were recorded.

Synthesis. The complexes [Cp*Ir(bpy)(Cl)][Cl] (**1Cl**), [(cymene)Ru(bpy)(Cl)][Cl] (**4Cl**), [(C$_6$Me$_6$)Ru(bpy)(Cl)][Cl] (**5Cl**), [Cp*Ir(bpy-Me)(Cl)][Cl] (**6Cl**), and [Cp*Ir(bpy-OMe)-(Cl)][Cl] (**7Cl**) were prepared following the method of Dadci et al., with final precipitation from MeOH/ether.[57] [Cp*Ir(Cl)$_2$]$_2$,[58] [Cp*Ir(bpy-COOH)(Cl)][Cl],[34] and [Cp*Ir(bpy)(H)][OTf][47] were prepared following literature procedures. [Cp*Ir(bpy)(OH$_2$)][SO$_4$][27] (**1OH$_2$**), [Cp*Ir(bpy-COOH)(OH$_2$)][OTf]$_2$,[59] (**2OH$_2$**), and [(cymene)Ru(bpy-COOH)(OH$_2$)][OTf]$_2$[46] (**3OH$_2$**) were prepared following literature procedures with the appropriate silver salt.

*[Cp*Ir(bpy-COO)(H)]$^-$ (2H) and [Cp*Ir(bpy-COO)]$^{2-}$ (2).* Electrolysis of **2Cl** in NaP$_i$, Na$_2$SO$_4$, or NaOH electrolytes (depending on the desired use of the product) past the first reduction feature (~ −1.0 V) resulted in conversion to reduced products, consistent with previously reported spectroscopic and electrochemical properties.[30] The form of these products (either **2H** or **2**) was highly dependent on solution pH, giving **2H** at neutral pH, **2** at high pH, and a mixture in between. To confirm the identities of these reduced products, **2Cl** (9.3 mg, 0.014 mmol) was reduced by excess NaBH$_4$ (3.7 mg, 0.98 mmol) by stirring for 30 min in MeOH. Filtration and evaporation produced a dark brown film. Dissolution in neutral water provided **2H**, and dissolution in basic water provided **2**. **2H**: ^{1}H NMR (600 MHz, D$_2$O + dioxane) δ 8.69 (d, J = 5.9 Hz, 2H), 8.55 (s, 2H), 7.72 (d, J = 5.9 Hz, 2H), 1.77 (s, 15H), −11.90 (s, 1H). $\lambda_{abs,max}$ (pH 7 0.1 M NaP$_i$) = 428 nm (3700 M^{-1} cm^{-1}). **2**: ^{1}H NMR (400 MHz, D$_2$O + dioxane) δ 8.81 (d, J = 7.0 Hz, 1H), 8.42 (s, 1H), 6.82 (dd, J = 6.9, 2.0 Hz, 1H). 1.80 (s, 15 H). $\lambda_{abs,max}$ (1 M NaOH) = 292 nm (22 000 M^{-1} cm^{-1}), 364 nm (10 800 M^{-1} cm^{-1}), 535 nm (23 000 M^{-1} cm^{-1}).

[(Cymene)Ru(bpy-COOH)(Cl)][Cl] (3Cl). Under nitrogen, [(cymene)RuCl$_2$]$_2$ (50.3 mg, 0.082 mmol) and bpy-COOH (40.3

mg, 0.165 mmol) were allowed to stir in 8 mL DMF at 60 °C for 3 h. After filtering the solution in air to remove unreacted ligand, the DMF was removed in vacuo. The resulting film was dissolved in MeOH, and yellow **3Cl** (83.4 mg, 92% yield) precipitated from solution on addition of ether. The ^{1}H NMR spectrum matched the previously reported data.[46]

[(Cymene)Ru(bpy-COO)(H)]$^-$ (3H) and [(cymene)Ru(bpy-COO)]$^{2-}$ (3). The hydride **3H** and reduced complex **3** were prepared according to the procedures for **2H** and **2**. **3H**: ^{1}H NMR (600 MHz, D$_2$O + dioxane) δ 8.87 (d, J = 5.8 Hz, 2H), 8.53 (d, J = 1.5 Hz, 2H), 7.64 (dd, J = 5.9, 1.6 Hz, 2H), 5.70 (d, J = 6.2 Hz, 2H), 5.51 (d, J = 6.1 Hz, 2H), 2.63 (sept, J = 6.9 Hz, 1H), 2.24 (s, 3H), 1.07 (d, J = 6.9 Hz, 6H), −6.21 (s, 1H). $\lambda_{abs,max}$ (pH 7 0.1 M NaP$_i$) = 295 nm (20 800 M^{-1} cm^{-1}), 434 nm (5500 M^{-1} cm^{-1}). **3**: ^{1}H NMR (600 MHz, D$_2$O + dioxane) δ 8.82 (d, J = 6.8 Hz, 2H), 8.37 (s, 2H), 7.12 (d, J = 6.7 Hz, 2H), 4.84 (d, J = 5.5 Hz, 2H), 4.81 (d, J = 5.7 Hz, 2H), 2.32 (sept, J = 7.7 Hz, 1H), 1.85 (s, 3H), 0.86 (d, J = 6.7 Hz, 6H). $\lambda_{abs,max}$ (1 M NaOH) = 298 nm (22 600 M^{-1} cm^{-1}), 374 nm (13 500 M^{-1} cm^{-1}), 506 nm (17 600 M^{-1} cm^{-1}), 610 nm (14 400 M^{-1} cm^{-1}).

*Cp*Ir(bpy) (1).* In a nitrogen filled glovebox, [Cp*Ir(bpy)(Cl)][Cl] (15.5 mg, 0.028 mmol) and excess NaBH$_4$ (8.5 mg, 0.223 mmol) were allowed to stir in 2 mL of 1 M NaOH. Dark purple solids quickly formed. After letting stir for 4 h, the solid was filtered off, washed 3× with water, collected in benzene, and evaporated to dryness, yielding **1** (13.3 mg, 98% yield). The ^{1}H NMR spectrum of **1** prepared in this way matched previously reported data.[60]

*[Cp*Ir(bpy)(H)][Cl] (1H).* To a stirring solution of **1** (13.3 mg, 0.028 mmol) in ether, a dilute solution of HCl·Et$_2$O (40 mM) was added dropwise until a change from a dark purple solution to bright yellow solids was observed. Typically 1−1.5 equiv of HCl was added with the excess acid immediately pumped off after completion of the addition. Samples of hydride prepared in this way typically contained small amounts (<5%) of [Cp*Ir(bpy)(Cl)][Cl] (formed by protonation of hydride releasing H$_2$), and the ^{1}H NMR spectrum is consistent with previously reported [Cp*Ir(bpy)(H)]$^+$.[30]

(Cymene)Ru(bpy) (4). Deep purple **4** was prepared in quantitative yield from the chloride salt of **4Cl**, according to the procedure used in the synthesis of **1**. The ^{1}H NMR spectrum matched the previously reported data.[61]

[(Cymene)Ru(bpy)(H)][Cl] (4H). The chloride salt of **4H** was prepared from **4**, according to the procedure used in the synthesis of the chloride salt of **1H**. ^{1}H NMR (600 MHz, D$_2$O + dioxane) δ 8.78 (d, J = 4.1 Hz, 2H), 8.09 (d, J = 8.2 Hz, 2H), 7.87 (t, J = 7.8 Hz, 2H), 7.32 (dd, J = 7.3, 5.8 Hz, 2H), 5.56 (d, J = 6.0 Hz, 2H), 5.36 (d, J = 6.0 Hz, 2H), 2.53 (sept, J = 7.1 Hz, 1H), 2.10 (s, 3H), 0.99 (d, J = 6.9 Hz, 6H), −6.32 (s, 1H).

(C$_6$Me$_6$)Ru(bpy) (5). Deep purple **5** was prepared in quantitative yield from the chloride salt of **5Cl**, according to the procedure used in the synthesis of **1**. The ^{1}H NMR spectrum matched the previously reported data.[61]

[(C$_6$Me$_6$)Ru(bpy)(H)][Cl] (5H). The chloride salt of **5H** was prepared from **5**, according to the procedure used in the synthesis of the chloride salt of **1H**. The ^{1}H NMR spectrum is consistent with the reported spectrum for the triflate salt of **5H** in water.[62]

*Cp*Ir(bpy-Me) (6).* In a nitrogen filled glovebox, [Cp*Ir(bpy-Me)(Cl)][Cl] (5.8 mg, 0.010 mmol) and excess NaBH$_4$ (5.1 mg, 0.135 mmol) were allowed to stir in 2 mL of 5 M NaOH, and a dark violet solid quickly formed. After letting stir for 4 h, the solid was extracted into C$_6$H$_6$, dried over MgSO$_4$, and evaporated to dryness, yielding **6** in quantitative yield. ^{1}H NMR (600 MHz, C$_6$D$_6$) δ 8.91 (d, J = 6.8 Hz, 2H), 7.44 (s, 2H), 6.06 (dd, J = 6.8, 2.1 Hz, 2H), 2.02 (s, 6H), 1.82 (s, 15H). ^{13}C NMR (151 MHz, C$_6$D$_6$) δ 148.20, 141.06, 127.59, 122.82, 117.92, 83.32, 21.44, 10.24. $\lambda_{abs,max}$ (C$_6$H$_6$) = 499, 641, 687 nm.

*[Cp*Ir(bpy-Me)(H)][Cl] (6H).* The bright yellow chloride salt of **6H** was prepared from **6**, according to the procedure used in the synthesis of the chloride salt of **1H**. ^{1}H NMR (600 MHz, D$_2$O + dioxane) δ 8.55 (d, J = 5.8 Hz, 2H), 7.91 (s, 2H), 7.32 (d, J = 6.0 Hz, 2H), 2.51 (s, 6H), 1.75 (s, 15H), −11.51 (s, 1H). $\lambda_{abs,max}$ (pH 7 0.1 M NaP$_i$) = 394 nm (2900 M^{-1}·cm^{-1}).

[Cp*Ir(bpy-OMe)(H)]⁺ (7H). Controlled potential electrolysis of $[Cp^*Ir(bpy\text{-}OMe)(Cl)][Cl]$ at −1.0 V in 0.1 M pD 7 NaP$_i$ resulted in clean formation of $[Cp^*Ir(bpy\text{-}OMe)(H)]^+$, consistent with previously reported spectroscopic and electrochemical properties.[30] ^{1}H NMR (600 MHz, D$_2$O + dioxane) δ 8.49 (d, J = 6.5 Hz, 2H), 7.44 (s, 2H), 7.06 (dd, J = 6.6, 2.8 Hz, 2H), 3.98 (s, 6H), 1.75 (s, 15H), −11.23 (s, 1H).

Cp*Ir(bpy-COOMe) (8). In a nitrogen filled glovebox, 8.1 mg (0.012 mmol) $[Cp^*Ir(bpy\text{-}COOMe)(Cl)][Cl]$ and 4.7 g (0.069 mmol) NaO$_2$CH were stirred in 2 mL pH 7 0.1 M NaP$_i$. While stirring for 4 h, a royal purple solid precipitated from solution. The solution was filtered, and the solids were washed 3× with water, collected by dissolving in benzene, and evaporated under vacuum to yield **8** (3.4 mg, 47% yield). ^{1}H NMR (600 MHz, C$_6$D$_6$) δ 8.78 (d, J = 7.0 Hz, 1H), 8.69 (d, J = 2.1 Hz, 1H), 7.20 (dd, J = 7.0, 2.0 Hz, 1H), 3.52 (s, 2H), 1.55 (s, 6H). ^{13}C NMR (151 MHz, C$_6$D6) δ 166.76, 147.22, 142.02, 125.72, 120.11, 115.04, 85.57, 51.76, 9.68. $λ_{abs,max}$ (C$_6$H$_6$) = 328, 389, 552 nm.

[Cp*Ir(bpy-COOMe)(H)][Cl] (8H). The scarlet chloride salt of **8H** was prepared from **8**, according to the procedure used in the synthesis of the chloride salt of **1H**. ^{1}H NMR (600 MHz, D$_2$O + dioxane) δ 8.89 (d, J = 5.9 Hz, 2H), 8.69 (s, 2H), 7.92 (d, J = 5.9 Hz, 2H), 4.10 (s, 6H), 1.80 (s, 15H), −12.28 (s, 1H). ^{13}C NMR (151 MHz, D$_2$O) δ 165.82, 155.95, 153.00, 138.06, 126.69, 123.19, 92.70, 54.39, 8.94. $λ_{abs,max}$ (pH 3 0.1 M NaP$_i$) = 388 nm (4200 M^{-1}·cm^{-1}), 451 nm (4300 M^{-1}·cm^{-1}), 481 nm (4400 M^{-1}·cm^{-1}).

Thermodynamic Measurements. *Hydride Equilibrations.* In a typical equilibration experiment to determine relative hydricity according to Figure 1B, 19.3 mg of **2Cl** was dissolved by sonication in 2 mL of pD 7 0.1 NaP$_i$, added to the working electrode compartment of an H-cell, and degassed for 15 min. The counter electrode compartment was charged with 2 mL pD 7 0.1 NaP$_i$. The solution was electrolyzed at −1.0 V for 6 h, transferred to a N$_2$ purged bomb flask, and brought into a glovebox. Different volumes of the electrolyzed solution (100, 200, and 300 μL) were added to three samples containing 3.5 mmol **1Cl** and dioxane, and the total volume was brought to 500 μL. Samples were monitored by ^{1}H NMR, and equilibrium of the experimental samples was quickly achieved; though the samples were monitored over 25 h by ^{1}H NMR, equilibrium (K_{eq} = 0.35) was established by the first time point, giving $ΔΔG°_{H^-}$ = 0.6 ± 0.1 kcal·mol^{-1}.

Alternatively, following protonation with HCl·Et$_2$O, the solid hydride was extracted into the NMR solvent (either pD 7 0.1 M NaP$_i$ or pD 4.3 20 mM NaOAc with dioxane internal standards), filtered to remove any residual Cp*Ir(bpy-X) or (arene)Ru(bpy-X), and combined with a hydride acceptor. Equilibration was followed by ^{1}H NMR. In a representative experiment, 2.0 mg of $[Cp^*Ir(bpy)(H)][Cl]$ (0.004 mmol) was dissolved in 490 μL of pD 7 0.1 M NaP$_i$ with 10 μL of 0.5 M dioxane as an internal standard. After confirming the purity of the hydride sample by ^{1}H NMR, 2.1 mg $[Cp^*Ir(bpy\text{-}Me)(Cl)][Cl]$ (0.004 mmol) was added to the NMR tube as a solid. $ΔΔG°_{H^-}$ was determined to be 0.4 ± 0.1 kcal·mol^{-1}.

Aquo-Chloride Association Equilibria. For each species, a series solutions of a known concentration of chloride were prepared in pD 7 NaP$_i$ and monitored by NMR to ensure that the aquo, phosphate, and chloride species were in equilibrium. For example, In air, a 5.5 mM solution of $[Cp^*Ir(bpy\text{-}COOH)(OH_2)][OTf]_2$ in 50 mM pD 7 NaP$_i$ with a dioxane internal standard was split between six samples each containing dry NaCl to produce final solutions with [Cl$^-$] from 0 to 18 mM. The samples were monitored by ^{1}H NMR over 24 h to ensure that equilibrium had been established between $[Cp^*Ir(bpy\text{-}COO)(OH_2)]^0$, [Cl$^-$] and $[Cp^*Ir(bpy\text{-}COO)(Cl)]^-$. The initial [Cl$^-$] left from the halide abstraction with AgOTf was fit by minimizing the variance of ΔG of the 0 mM NaCl added sample with that of the remaining five samples. The free energy of the ligand exchange was found to be −4.4 ± 0.2 kcal·mol^{-1}. The relative aquo-phosphate association free energy was determined similarly with solutions of increasing total [P$_i$] at pD 7.

■ AUTHOR INFORMATION

Corresponding Author

*ajmm@email.unc.edu

Notes

The authors declare no competing financial interest.

■ REFERENCES

(1) Vincent, K. A.; Parkin, A.; Armstrong, F. A. *Chem. Rev.* **2007**, *107*, 4366−4413.

(2) Dobbek, H.; Svetlitchnyi, V.; Gremer, L.; Huber, R.; Meyer, O. *Science* **2001**, *293*, 1281−1285.

(3) Gray, H. B. *Nat. Chem.* **2009**, *1*, 112−112.

(4) Thoi, V. S.; Sun, Y.; Long, J. R.; Chang, C. J. *Chem. Soc. Rev.* **2013**, *42*, 2388−2400.

(5) McDaniel, N. D.; Bernhard, S. *Dalton Trans.* **2010**, *39*, 10021−10030.

(6) Appel, A. M.; Bercaw, J. E.; Bocarsly, A. B.; Dobbek, H.; DuBois, D. L.; Dupuis, M.; Ferry, J. G.; Fujita, E.; Hille, R.; Kenis, P. J. A.; Kerfeld, C. A.; Morris, R. H.; Peden, C. H. F.; Portis, A. R.; Ragsdale, S. W.; Rauchfuss, T. B.; Reek, J. N. H.; Seefeldt, L. C.; Thauer, R. K.; Waldrop, G. L. *Chem. Rev.* **2013**, *113*, 6621−6658.

(7) *Aqueous-Phase Organometallic Catalysis*, 2nd ed.; Cornils, B., Herrmann, W. A., Eds.; Wiley-VCH: Weinheim, 2004.

(8) Joó, F. *Acc. Chem. Res.* **2002**, *35*, 738−745.

(9) Volbeda, A.; Charon, M.-H.; Piras, C.; Hatchikian, E. C.; Frey, M.; Fontecilla-Camps, J. C. *Nature* **1995**, *373*, 580−587.

(10) Peters, J. W.; Lanzilotta, W. N.; Lemon, B. J.; Seefeldt, L. C. *Science* **1998**, *282*, 1853−1858.

(11) Han, Z.; Eisenberg, R. *Acc. Chem. Res.* **2014**, *47*, 2537−2544.

(12) Warren, J. J.; Tronic, T. A.; Mayer, J. M. *Chem. Rev.* **2010**, *110*, 6961−7001.

(13) Bourrez, M.; Steinmetz, R.; Ott, S.; Gloaguen, F.; Hammarström, L. *Nat. Chem.* **2015**, *7*, 140−145.

(14) DuBois, D. L.; Berning, D. E. *Appl. Organomet. Chem.* **2000**, *14*, 860−862.

(15) Rakowski DuBois, M.; DuBois, D. L. *Chem. Soc. Rev.* **2009**, *38*, 62−72.

(16) Bullock, R. M.; Appel, A. M.; Helm, M. L. *Chem. Commun.* **2014**, *50*, 3125−3143.

(17) Helm, M. L.; Stewart, M. P.; Bullock, R. M.; Rakowski DuBois, M.; Dubois, D. L. *Science* **2011**, *333*, 863−866.

(18) Rodriguez-Maciá, P.; Dutta, A.; Lubitz, W.; Shaw, W. J.; Rüdiger, O. *Angew. Chem., Int. Ed.* **2015**, *54*, 12303−12307.

(19) Connelly, S. J.; Wiedner, E. S.; Appel, A. M. *Dalton Trans.* **2015**, *44*, 5933−5938.

(20) Creutz, C.; Chou, M. H. *J. Am. Chem. Soc.* **2007**, *129*, 10108−10109.

(21) Creutz, C.; Chou, M. H. *J. Am. Chem. Soc.* **2009**, *131*, 2794−2795.

(22) Taheri, A.; Thompson, E. J.; Fettinger, J. C.; Berben, L. A. *ACS Catal.* **2015**, *5*, 7140−7151.

(23) Tsay, C.; Livesay, B. N.; Ruelas, S.; Yang, J. Y. *J. Am. Chem. Soc.* **2015**, *137*, 14114−14121.

(24) See the Supporting Information for full details.

(25) Berning, D. E.; Noll, B. C.; DuBois, D. L. *J. Am. Chem. Soc.* **1999**, *121*, 11432−11447.

(26) Brewster, T. P.; Miller, A. J. M.; Heinekey, D. M.; Goldberg, K. I. *J. Am. Chem. Soc.* **2013**, *135*, 16022−16025.

(27) Miller, A. J. M.; Heinekey, D. M.; Mayer, J. M.; Goldberg, K. I. *Angew. Chem., Int. Ed.* **2013**, *52*, 3981−3984.

(28) Hull, J. F.; Himeda, Y.; Wang, W.-H.; Hashiguchi, B.; Periana, R.; Szalda, D. J.; Muckerman, J. T.; Fujita, E. *Nat. Chem.* **2012**, *4*, 383−388.

(29) Fukuzumi, S.; Kobayashi, T.; Suenobu, T. *Angew. Chem., Int. Ed.* **2011**, *50*, 728−731.

(30) Pitman, C. L.; Miller, A. J. M. *ACS Catal.* **2014**, *4*, 2727−2733.

(31) Himeda, Y. *Green Chem.* **2009**, *11*, 2018−2022.

(32) Ogo, S.; Kabe, R.; Hayashi, H.; Harada, R.; Fukuzumi, S. *Dalton Trans.* **2006**, *39*, 4657−4663.

(33) Taheri, A.; Berben, L. A. *Inorg. Chem.* **2016**, *55*, 378−385.

(34) Ziessel, R. *J. Am. Chem. Soc.* **1993**, *115*, 118−127.

(35) Dutton, L. P. *Methods Enzymol.* **1978**, *54*, 411−435.

(36) Pugh, J. R.; Meyer, T. J. *J. Am. Chem. Soc.* **1992**, *114*, 3784−3792.

(37) Seifriz, I.; Konzen, M.; Paula, M. M. S.; Gonçalves, N. S.; Spoganickz, B.; Creczynski-Pasa, T. B.; Bonetti, V. R.; Beirith, A.; Calixto, J. B.; Franco, C. V. *J. Inorg. Biochem.* **1999**, *76*, 153−163.

(38) Ardo, S.; Achey, D.; Morris, A. J.; Abrahamsson, M.; Meyer, G. J. *J. Am. Chem. Soc.* **2011**, *133*, 16572−16580.

(39) Ciancanelli, R.; Noll, B. C.; DuBois, D. L.; Rakowski DuBois, M. *J. Am. Chem. Soc.* **2002**, *124*, 2984−2992.

(40) Wilson, A. D.; Miller, A. J. M.; DuBois, D. L.; Labinger, J. A.; Bercaw, J. E. *Inorg. Chem.* **2010**, *49*, 3918−3926.

(41) Matsubara, Y.; Fujita, E.; Doherty, M. D.; Muckerman, J. T.; Creutz, C. *J. Am. Chem. Soc.* **2012**, *134*, 15743−15757.

(42) Hu, Y.; Norton, J. R. *J. Am. Chem. Soc.* **2014**, *136*, 5938−5948.

(43) Kolthoff, I. M. *Anal. Chem.* **1974**, *46*, 1992−2003.

(44) Five-coordinate d^8 transition metal hydrides have been a focus of studies in MeCN. Solvent ligation is minimized in these cases because the product of hydride transfer is d^8 square planar. See ref 15.

(45) Robertson, A.; Matsumoto, T.; Ogo, S. *Dalton Trans.* **2011**, *40*, 10304−10310.

(46) de Respinis, M.; Joya, K. S.; De Groot, H. J. M.; D'Souza, F.; Smith, W. A.; van de Krol, R.; Dam, B. *J. Phys. Chem. C* **2015**, *119*, 7275−7281.

(47) Barrett, S. M.; Pitman, C. L.; Walden, A. G.; Miller, A. J. M. *J. Am. Chem. Soc.* **2014**, *136*, 14718−14721.

(48) Ellis, W. W.; Miedaner, A.; Curtis, C. J.; Gibson, D. H.; DuBois, D. L. *J. Am. Chem. Soc.* **2002**, *124*, 1926−1932.

(49) Bhagan, S.; Wayland, B. B. *Inorg. Chem.* **2011**, *50*, 11011−11020.

(50) Curtis, C. J.; Miedaner, A.; Ellis, W. W.; DuBois, D. L. *J. Am. Chem. Soc.* **2002**, *124*, 1918−1925.

(51) Hansch, C.; Leo, A.; Taft, R. W. *Chem. Rev.* **1991**, *91*, 165−195.

(52) Kanan, M. W.; Nocera, D. G. *Science* **2008**, *321*, 1072−1075.

(53) Karunadasa, H. I.; Chang, C. J.; Long, J. R. *Nature* **2010**, *464*, 1329−1333.

(54) Fulmer, G. R.; Miller, A. J. M.; Sherden, N. H.; Gottlieb, H. E.; Nudelman, A.; Stoltz, B. M.; Bercaw, J. E.; Goldberg, K. I. *Organometallics* **2010**, *29*, 2176−2179.

(55) Glasoe, P. K.; Long, F. A. *J. Phys. Chem.* **1960**, *64*, 188−190.

(56) *Handbook of Electrochemistry*; Zoski, C. G., Ed.; Elsevier: Amsterdam, 2007.

(57) Dadci, L.; Elias, H.; Frey, U.; Hoernig, A.; Koelle, U.; Merbach, A. E.; Paulus, H.; Schneider, J. S. *Inorg. Chem.* **1995**, *34*, 306−315.

(58) White, C.; Yates, A.; Maitlis, P. M. *Inorg. Synth.* **1992**, *29*, 228−234.

(59) Joya, K. S.; Subbaiyan, N. K.; D'Souza, F.; de Groot, H. J. M. *Angew. Chem., Int. Ed.* **2012**, *51*, 9601−9605.

(60) Ladwig, M.; Kaim, W. *J. Organomet. Chem.* **1992**, *439*, 79−90.

(61) Kaim, W.; Reinhardt, R.; Sieger, M. *Inorg. Chem.* **1994**, *33*, 4453−4459.

(62) Ogo, S.; Uehara, K.; Abura, T.; Watanabe, Y.; Fukuzumi, S. *Organometallics* **2004**, *23*, 3047−3052.